Cells and Materials

Volume 5 | Number 3 Article 6

1995

Backscattered Electron Imaging to Enhance Microstructural Contrast in Poly(Methyl Methacrylate) Bone Cement Fracture Analysis

L. D. T. Topoleski
University of Maryland Baltimore County

P. Rutledge
University of Maryland Baltimore County

X. Lu
University of Maryland Baltimore County

Cells and Materials, Vol. 5, No. 3, 1995 (Pages 283-292) 0891-7035/95$5.00+.25
Scanning Microscopy International, Chicago (AMF O'Hare), IL 60666 USA

BACKSCATTERED ELECTRON IMAGING TO ENHANCE MICROSTRUCTURAL CONTRAST IN POLY(METHYL METHACRYLATE) BONE CEMENT FRACTURE ANALYSIS

L.D.T. Topoleski*, P. Rutledge[1], and X. Lu

[1]Department of Mechanical Engineering and [2]Department of Biological Science,
University of Maryland Baltimore County, Baltimore, MD 21228

(Received for publication June 9, 1995 and in revised form November 30, 1995)

Abstract

Poly(methyl methacrylate) (PMMA) bone cement is used as a grout to secure joint replacement prostheses into bone. It has a distinct microstructure made up of: prepolymerized beads, an interbead matrix polymer, a radiopacifier {barium sulphate ($BaSO_4$) or zirconium dioxide (ZrO_2)}, and pores or voids; the radiopacifier is found only in the interbead matrix of the cured bone cement. The mechanism of slow or fatigue crack growth appears to be initial micro-cracking through the interbead matrix, followed by coalescence of the microcracks to form a continuous crack. Thus, distinguishing the interbead matrix from the pre-polymerized beads is important for investigating fatigue crack behavior in bone cement. Backscattered electron (BE) imaging theoretically facilitates discrimination of the radiopacifier, and thus, interbead matrix polymer, from the prepolymerized beads. The purpose of this study was to investigate the use of BE imaging and secondary electron (SE) imaging to enhance the contrast between the microstructural components in PMMA bone cement. Electron microscopy revealed that: (1) the damage zone in fatigue fracture of PMMA was characterized by microcracks ahead of the crack tip, and (2) in the BE micrographs, it was easy to differentiate the prepolymerized beads from the interbead matrix. Therefore, BE imaging can be successfully used to contrast the radiopacifier with other constituents of the cement.

Key Words: Scanning electron microscopy, backscattered electron imaging, bone cement, fracture, fatigue, microstructure, biomaterials, joint replacement.

*Address for correspondence:
L.D.T. Topoleski
Department of Mechanical Engineering,
University of Maryland Baltimore County,
5401 Wilkens Avenue, Baltimore, MD 21228.
Telephone number: (410) 455-3302
FAX number: (410) 455-1052
E.mail: Topoleski@umbc2.umbc.edu

Introduction

Poly(methyl methacrylate) (PMMA) based bone cement may be the most commonly implanted non-metallic biomaterial. PMMA was introduced by Charnley [4] predominantly as a grout to secure joint replacement prostheses into bone. Some of the most important factors influencing the success of a total joint prosthesis are physiological stress transfer from the prosthesis to the bone, maintaining the mechanical integrity of the prosthesis (avoiding material fracture), and maintaining the integrity of the surrounding bone (avoiding osteolysis). Physiological stress transfer requires intact metal/bone cement and bone/bone cement interfaces, and therefore, the mechanical properties and failure resistance of PMMA are an integral part of any cemented prosthetic system. To increase the longevity of prostheses, modifications of the cemented system have been suggested and implemented, including eliminating bone cement altogether, and making use of biological fixation [6, 7, 8, 9, 10, 15], strengthening the bone cement (by porosity reduction or adding reinforcing fibers) [3, 5, 11, 16, 17, 18, 19, 20, 22, 24, 26, 27], or modifying the chemical composition [14, 25].

PMMA bone cement has the same chemical composition as the acrylics commercially known as Plexiglas®, Lucite®, or Perspex®. In contrast to commercial grade PMMA, which is a homogeneous material polymerized under controlled conditions, PMMA bone cement has a distinct microstructure. The principal microstructural components of orthopaedic bone cement are: prepolymerized PMMA beads (or beads of a related copolymer), an interbead matrix polymer created by polymerization of methyl methacrylate (MMA) monomer as the bone cement is mixed, a radiopacifier {usually barium-sulphate ($BaSO_4$) or zirconium dioxide (ZrO_2)}, and pores or voids (Figure 1).

The radiopacifier is found only in the interbead matrix of the cured bone cement. The mechanism of slow or fatigue crack growth appears to be initial microcracking through the interbead matrix, followed by coalescence of the microcracks to form a continuous crack

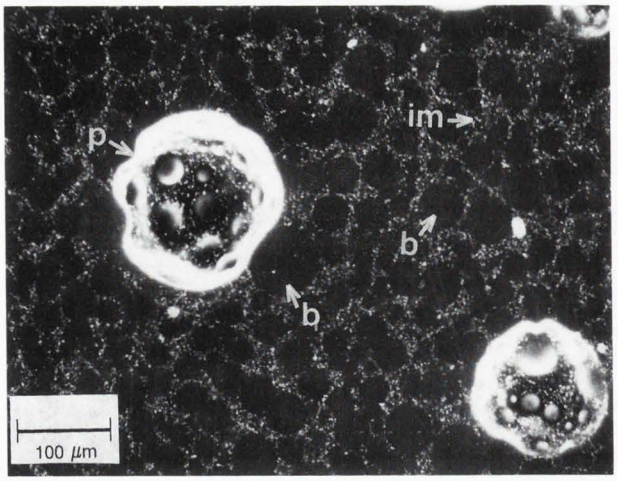

Figure 1. The components of bone cement microstructure. The PMMA beads, from the packaged powder (b) are seen as dark circles. The interbead matrix (im) is the lighter material surrounding the beads; the lighter color is created by the $BaSO_4$ radiopacifier. Pores of over 100 μm in diameter (p) are often found in cured bone cement.

---

[23]. The presence of the radiopacifier in the interbead matrix may be the reason for the microcracking. Thus, distinguishing the interbead matrix from the pre-polymerized beads is important and necessary for investigating the fatigue crack behavior in PMMA bone cement.

Previous investigators have been able to discern interbead matrix and pre-polymerized beads using standard secondary electron (SE) imaging [1, 12, 13, 23, 27]; however, depending on the type of sample, the thickness of the conductive coating applied to the sample, electron beam spot size, aperture, electron accelerating voltage, and other factors, the distinction is not always clear. Because of the difference in atomic number of elements such as barium or zirconium, compared to the carbon, hydrogen, and oxygen of PMMA, backscattered electron (BE) imaging should theoretically facilitate discrimination of the radiopacifier (and thus, interbead matrix polymer) from the prepolymerized beads by virtue of the so-called Z contrast [2].

The purpose of this study was to investigate the use of BE and SE images to enhance the contrast between the microstructural components in PMMA bone cement. Then, the information discernable from the enhanced images was applied to investigate the mechanisms of fatigue crack initiation and propagation.

Methods and Materials

Bone cement (Simplex®, Howmedica, Inc. Rutherford, NJ) was mixed according to the package insert's instructions. Briefly, bone cement is packaged as two separate parts. The first, a powder of prepolymerized beads, also contains a radiopacifier and an initiator, usually benzoyl peroxide. In the specific formulation used in this study, an amorphous PMMA-polystyrene co-polymer powder is also admixed in the powder component. The second is a liquid MMA monomer, that contains an "activator" or "accelerator", usually dimethyl-p-toluidine, which activates the benzoyl peroxide. The monomer is added to the powder, and the polymerization reaction is initiated. The bone cement analyzed contained $BaSO_4$ as the radiopacifier.

The bone cement was injected into a specially designed mold for rectangular bar bending specimens (10 mm x 10 mm x 60 mm). Two types of notching methods were used. The first type of notch was cut using a low speed diamond blade. The resulting notch was "blunt", and a sharp notch tip was introduced using a scalpel (Figures 2a and 2b). The second type of notch was created by adapting the specimen mold to include either one or three razor blades which molded sharp notches into the curing bone cement (Figures 2c and 2d). Eleven single notched specimens (7 cut, 4 molded) and ten triple notched specimens (2 cut and 8 molded) were tested. The specimens were allowed to cure in the mold, at room temperature, for approximately one hour. If the notches were cut into the specimen, the cutting took place immediately after the specimens were removed from the mold. The specimens were then placed in Hank's balanced salt saline solution in an incubator at 37°C for at least 24 hours prior to testing.

The bone cement specimens were placed in a 4 point bending fixture and cyclically loaded ("fatigued") at 5 Hz on an MTS 858 Bionix test system. The loading range was from 25-125 N, resulting in a stress intensity (K_I) range of 0.0904-0.542 $MPa(m)^{1/2}$ for the initial notch length (3.81 mm). The maximum K_I was approximately one-third of the reported values for K_{IC} of bone cement [3, 17, 18, 22, 24]. An extensometer was attached to the specimen at the center notch to monitor crack opening displacement (COD), in order to determine whether a crack had initiated. Because the notch tips were extremely sharp, crack initiation occurred quickly, usually within 6,000 cycles.

The COD was monitored in the hope of detecting crack initiation from one of the notches. If a crack initiated at one of the notches, the other notches were essentially unloaded. In the four point bending configuration, the single crack continued to grow, theoretically, from only one notch. Crack initiation should have produced a change in the COD. The remaining notches will not have generated a crack, but retained evidence of the crack initiation process. In practice, it was difficult to detect the initial crack event, however, the COD

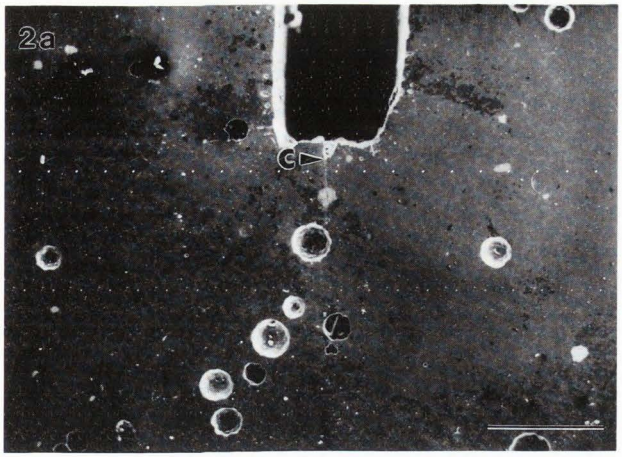

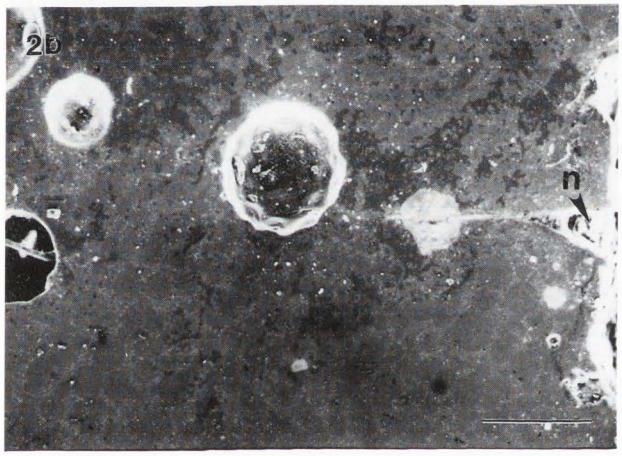

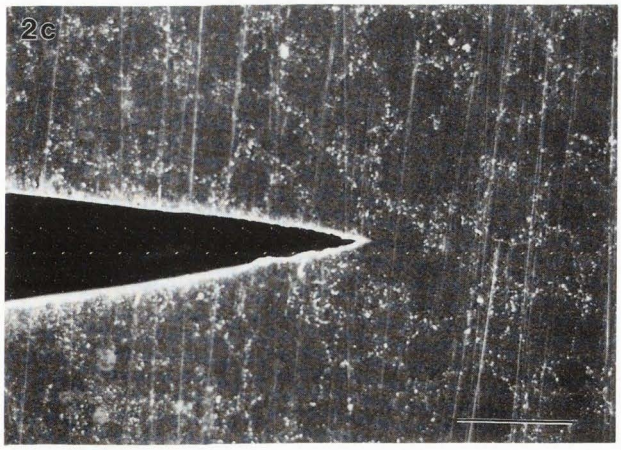

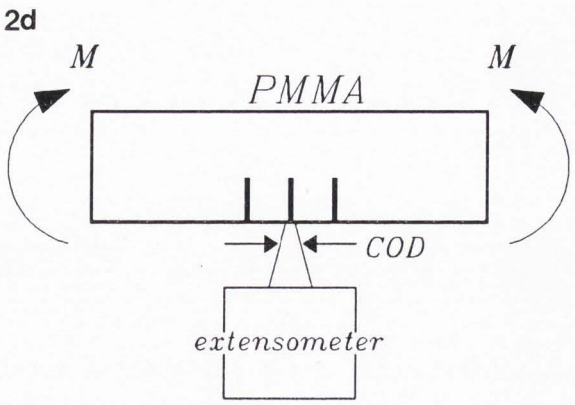

Figure 2. (**a, b and c**). SE images of: (**a**) a notch created by first cutting the specimen using a slow-speed diamond saw, then scoring with a scalpel to create a sharp tip; this specimen has already been tested and a crack (c) on the order of 600-700 μm long has initiated; (**b**) higher magnification of the same notch, rotated 90°; The tip of the saw blade cut is rough; the notch (n) often gets clogged with debris during polishing, which does not affect the crack behavior; and (**c**) a razor-blade-molded notch; the sides of the notch are smooth, and the notch tip radius is on the order of 3 μm. Molded notches were reproducible, and were used exclusively for fatigue crack initiation study when the diamond saw notches were deemed unreliable. In (**c**), the bead and interbead matrix are distinguishable. Bars = 1 mm (a), 300 μm (b) and 100 μm (c). (**d**). A schematic of a side view of the specimen showing the relative positions of the notches and the applied bending moment. If only one notch was incorporated into the specimen, it was centered.

monitoring technique proved useful for detecting developing cracks on the order of 10 μm long, and for observing initiation phenomena.

Once a crack was thought to have initiated, the specimen was removed from the testing apparatus. One side of the specimen was polished on a polishing wheel using sequentially smaller alumina powder slurries (1.0, 0.3, 0.05 μm). Polishing removed aberrations in the fracture that may have been caused by surface features, and were not relevant to the fracture processes in the bulk material. The polishing procedure removed approximately 1.5 mm of the specimen's surface. The ends of the specimens were then trimmed to better fit the specimen into the scanning electron microscope (SEM).

Both fatigued and non-fatigued control specimens were studied using a JEOL JSM 35CF SEM operated at accelerating voltages of 15-20 kV. A special mounting fixture was designed to place the specimen to be examined under bending loads, thus, opening the crack. The specimen was loaded by gently turning set screws to open the notches. COD during SEM preparation was monitored by the same extensometer used during fatigue testing. The notches were opened considerably less than they were during fatigue testing to avoid creating fracture artifacts. The control specimens (at least 3 for each

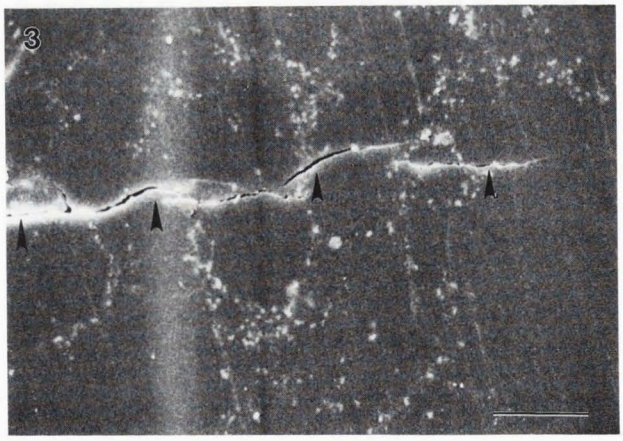

Figure 3. An SE image of a fatigue crack showing the discontinuity characteristic of the crack tip process zone. The crack is growing from left to right. In this micrograph, microcracks appear to grow preferentially in the interbead matrix. Microcrack coalescence occurs as the crack advances. Bar = 20 μm.

---

type of notching method) were prepared in the same way to determine whether artifacts were created during the preparation protocol.

The opened specimens were placed in a sputter-coater (Polaron E53000), and coated with approximately 10 nm of gold or gold-palladium. The coating was applied in three or four stages to avoid over-heating the polymer. The specimens were then placed in the SEM for both SE and BE imaging.

Results

Electron microscopy clearly revealed two features: (1) the damage zone in fatigue fracture of PMMA was characterized by microcracks ahead of the crack tip (Figure 3) as previously reported [23], and (2) in the BE micrographs, it was easy to differentiate the prepolymerized beads from the interbead matrix (Figure 4a).

The cracks that initiated from a prepared notch began propagating perpendicularly to the direction of the maximum tension (Figure 5a). In some cases, pores were serendipitously located near the line of the crack propagation. As the crack moved into the vicinity of a pore, it changed directions to intersect the pore before returning to its initial path (Figure 5b). The BE clearly showed that the crack actually propagated around a prepolymerized bead adjacent to the pore (through the interbead matrix) before intersecting the pore (Figure 5c).

In a section of propagation in a well established crack, the SE image showed that the crack diverted to intersect a pore before returning to its preferred path, propagating through an agglomerate of $BaSO_4$, and then

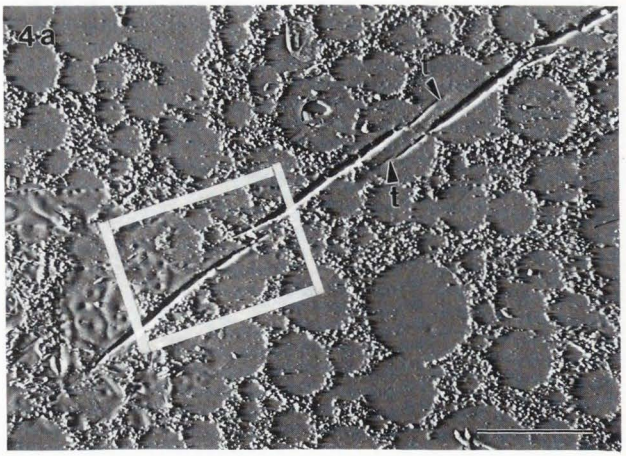

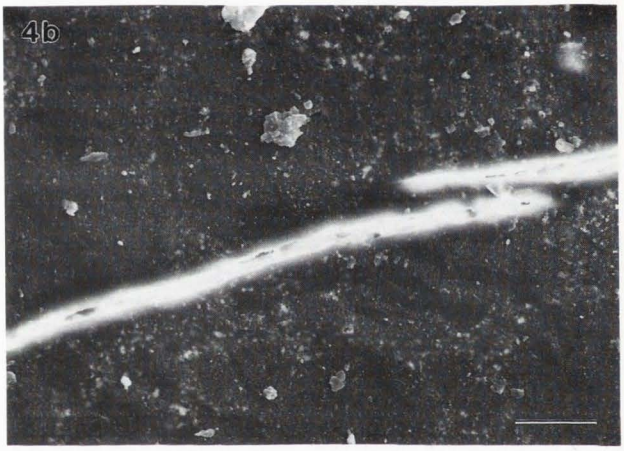

Figure 4. Microcracks growing through bone cement. (**a**). The BE image clearly differentiates the PMMA beads (circles in cross-section) from the $BaSO_4$ containing interbead matrix. Three disconnected "microcracks" are shown. The microcracks appear to have terminated within the PMMA beads (t). The pockmarks on the lower left of the micrograph were caused by beam damage while attempting to photograph at a higher magnification. Bar = 100 μm. (**b**). The SE image of the microcrack terminations indicated in Figure 4a, at a higher magnification. In this micrograph, it is nearly impossible to differentiate the pre-polymerized beads from the matrix. Bar = 30 μm.

---

diverting to a second pore (Figure 6a). The BE image showed that the crack again tended to propagate between the beads (Figure 6b) and also revealed that the crack apparently propagated into a bead and terminated, only to continue growing along an alternate path through the matrix. The crack propagation into the bead was not clear in the SE image.

Figure 5 (at right). BE and SE images showing a crack in the early stages of propagation in the vicinity of a pore. (**a**). SE image of the primary crack that has grown from the notch (n), which is difficult to see in detail because of charging. The main direction of propagation is indicated by the arrow. In general, the crack appears to have grown perpendicularly to the direction of the maximum principal stress (which occurs horizontally in the picture frame), until it approached the pore. The crack then took a "detour", intersected the pore, and returned to its original path. The discontinuous nature of the propagation is evident as the primary crack has not yet joined a microcrack that has opened at the bottom of the picture. Bar = 100 μm. (**b**). An enlargement of Figure 5a showing the top of the pore and the path of the crack that diverged to meet it. Bar = 10 mm. (**c**). A BE image corresponding to Figure 5b (the directional cross, "+", is at the same location in Figures 5b and 5c, and gives the relative orientation), showing that the crack actually propagated around a polymer bead when it was diverted to the pore, rather than taking the more direct route through the bead. Beam damage (d) is evident. The black arrowheads are pointing at the interbead matrix, and are directed radially outward from the center of several beads. Beads are identified by roughly circular areas lacking the bright white specks of the radiopacifier. Bar = 10 μm.

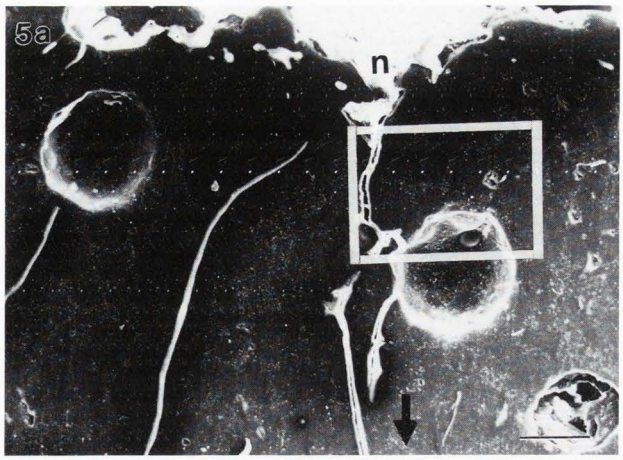

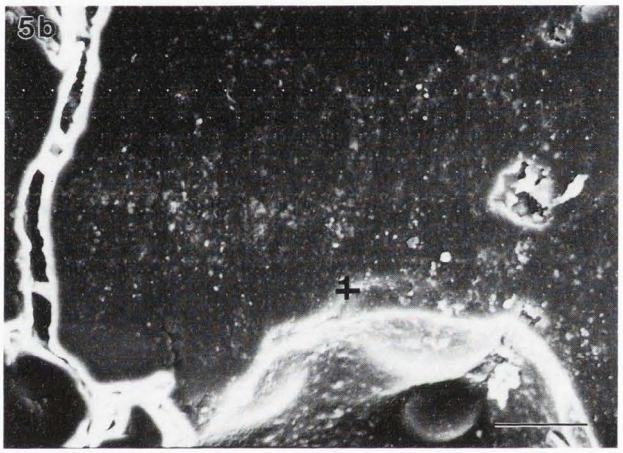

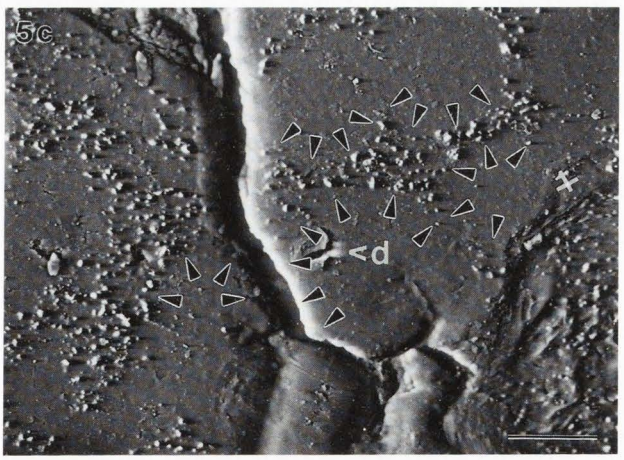

The method of creating the initial notch was observed to play an important role in the fatigue crack initiation process. The diamond saw-scalpel cut notches were inconsistent, and it was difficult to create reproducible geometries. The scalpel cut may have led to specimen damage, i.e., microcracking, thus, negating any study of crack initiation. The molded razor-blade notches were reproducible, and produced no initial microcracking.

Discussion

Because it was difficult to create consistent notches using the diamond saw, we abandoned that technique for studying **crack initiation** in bone cement. The microscopic data showing crack propagation, however, and the phenomena revealed by backscattered imaging are still tenable. Evaluation of the notching technique for fatigue crack initiation were not a part of this study, and are therefore not discussed further.

Cracks were generally distinguishable in the micrographs because there tended to be charging of the inner surface (Figure 4), despite coating with the crack opened by the special SEM fixture. The charging was somewhat fortuitous, because it did allow imaging of the extensive microcrack process zone associated with fatigue failure in bone cement. Crack charging had an unfavorable effect, however, obscuring some of the adjacent microstructural details. Because of the obvious contrast between the $BaSO_4$ (identifying the interbead matrix polymer), and the PMMA beads, BE images increased the ability to identify the material through which the cracks were propagating. Even in the polished and ultrasonically cleaned specimens, there was PMMA debris on the surfaces, which appeared white in SE images because of

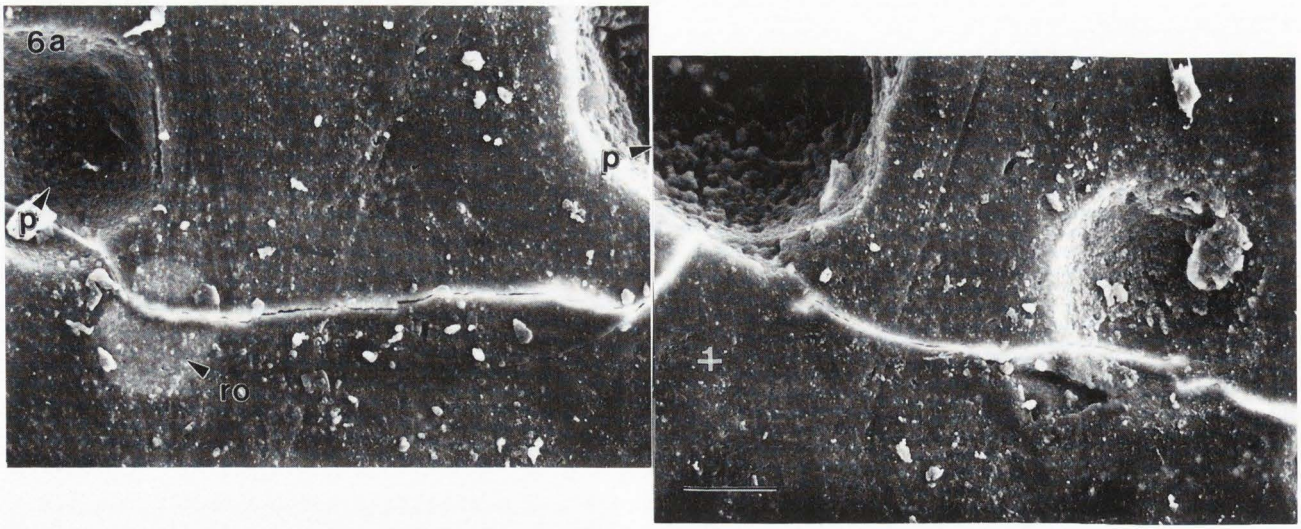

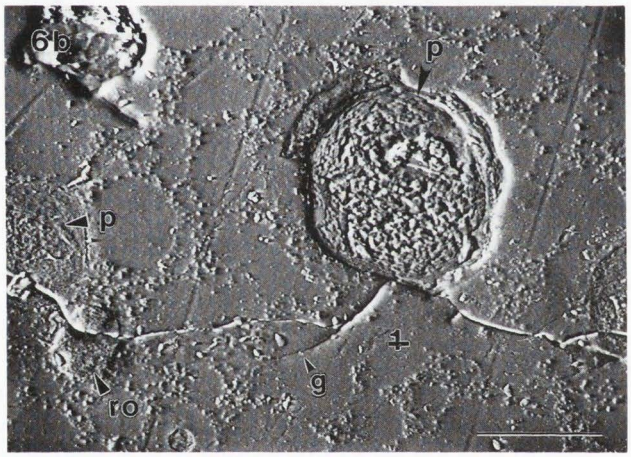

Figure 6. The propagation path of a well established crack. (**a**). An SE micrograph montage of the crack path. There again appears to be a preferred direction for crack propagation (the crack is propagating from right to left), which is perpendicular to the direction of the maximum principal stress in the specimen. The crack deviated from this preferred direction only to intersect nearby pores (p), and through an agglomerate of radiopacifier (ro). Bar = 30 μm. (**b**). The BE micrograph of the same crack (the directional cross, "+", is at the same location in Figures 6a and 6b, and gives the relative orientation) shows that the crack tended to propagate within the interbead matrix. It appears that the crack attempted to propagate in a reasonably straight line, which forced the crack tip to grow into a prepolymerized bead (g). The crack propagation in that direction terminated in favor of continued growth through the radiopacifier agglomerate (ro) and toward the pore (p). Bar = 100 μm.

charging. The Z contrast of BE image also eliminated mistaking PMMA debris for $BaSO_4$.

Both the SE and BE micrographs show that the cracks appeared discontinuous (Figure 4). Although the BE micrograph was taken at a lower magnification than the SE micrograph, it is easy to see that the individual microcracks appear to terminate within PMMA beads. That information was not discernable from the SE micrograph. Based on previous observations that the microcracks appear to propagate through the interbead matrix [21, 23], it is likely that the microcracks **initiated** in the interbead matrix. The microcracks progressed in both directions from the point of initiation, then terminated in the PMMA beads. The characteristic surface morphology of fatigue fracture in PMMA bone cements suggests that when the stresses become great enough, the microcracks eventually coalesce by PMMA bead fracture [21, 23].

These micrographs (Figure 6) show only a single cross-section of a fully three-dimensional fracture process. The crack, and the crack damage zone, extend through the specimen (into the plane of the micrographs). A full description of the crack extension process must therefore include the entire propagating crack; however, the discontinuous damage zone was observed to be independent of specimen polishing depth, and was present when specimens were sequentially polished and observed in the SEM.

The interaction between pores and the propagating crack (Figures 5 and 6) appeared to be short range. Pores caused deviations from a preferred crack path, but the crack soon recovered the original path. BE image (Figure 5c) showed that a single PMMA bead, approximately 60 μm in diameter, interfered with the crack's propagation path. The crack appeared to choose a path around the bead, growing through the interbead matrix, as a route toward intersecting a pore over 100 μm in

diameter, illustrating the short proximity of the pore's effect on the stress field of the crack. The BE image analysis enabled the isolation and observation of the interaction between the crack and a single bead adjacent to a pore.

Specimen damage from the electron beam was common during BE imaging. Because the images were difficult to focus, high magnification images were problematic, although with considerable care, some luck, and quick technical operation, higher magnification was used to produce useful BE images (see, e.g., Figure 4b). When a BE image was called for, e.g., to enhance the contrast of the microstructural constituents, an SE image was first produced because the conditions necessary to produce the BE image were most likely going to damage the specimen, and thus make a follow-up SE image worthless. Pairs of SE/BE images of the same area of the specimen were not likely to be centered exactly the same, because of the adjustments necessary to produce useful a BE image (e.g., see Figures 5b and 5c).

Conclusions

Backscattered electron imaging can be successfully used to contrast the radiopacifier constituent in PMMA bone cement with other polymer constituents and porosity. The BE image provides information that is not generally available from SE image. The microstructural distinction allows a more detailed investigation of the role that the constituents play in the fatigue failure of bone cement.

Acknowledgments

We are grateful to Howmedica, Inc. for a donation of some of the bone cement used in this study. The authors wish to thank the Arthritis Foundation for supporting this project; L.D.T. Topoleski is the recipient of an Arthritis Foundation Arthritis Investigator Award.

References

[1] Beaumont PWR (1977) The strength of acrylic bone cements and acrylic cement-stainless steel interfaces. Part 1. The strength of acrylic bone cement containing second phase dispersions. J. Mater. Sci. **12**: 1845-1852.

[2] Bozzola JJ, Russell LD (1992) Electron Microscopy, Principles and Techniques for Biologists. Jones and Bartlett, Boston. pp. 205-207.

[3] Burke DW, Gates EJ, Harris WH (1984) Centrifugation as a method of improving tensile and fatigue properties of acrylic bone cement. J. Bone Joint Surg. **66-A**: 1265-1273.

[4] Charnley J (1960) Anchorage of the femoral head prosthesis to the shaft of the femur. J. Bone Joint Surg. **42-B**: 28-30.

[5] Davies JP, O'Connor DO, Burke DW, Jasty M, Harris WH (1988) The effect of centrifugation on the fatigue life of bone cement in the presence of surface irregularities. Clin. Orthop. Rel. Res. **229**: 156-161.

[6] Ducheyne P, Hench LL, Kagen A, Martens M, Bursens A, Mulier JC (1980) Effect of hydroxyapatite impregnation on skeletal bonding of porous coated implants. J. Biomed. Mater. Res. **14**: 225-237.

[7] Galante J, Rostoker W, Lueck R, Ray RD (1971) Sintered fiber metal composites as a basis for attachment of implants to bone. J. Bone Joint Surg. **53A**: 101-114.

[8] Hansen LB, Kroman B, Baekgaard N (1986) Uncemented two-component femoral prosthesis for the hip joint. Clin. Orthop. Rel. Res. **206**: 182-187.

[9] Hench LL, Pantano CG, Buscemi PJ, Grenspan DC (1977) Analysis of bioglass fixation of hip prostheses. J. Biomed. Mater. Res. **11**: 267-232.

[10] Hench LL, Splinter RJ, Allen WC, Greenlee TK (1972) Bonding mechanisms at the interface of ceramic prosthetic materials. J. Biomed. Mater. Res. Symp. **2**: 117-141.

[11] Krause WR, Mathis RS, Grimes LW (1988) Fatigue properties of acrylic bone cement: S-N, P-N, and P-S-N data. J. Biomed. Mater. Res.: Appl. Biomat. **22**: 221-244.

[12] Kusy RP, Turner DT (1974) Intergranular cracking of a weak two-phase polymethyl methacrylate. J. Biomed. Mater. Res. **8**: 185-188.

[13] Kusy RP, Turner DT (1975) Fractography of poly(methylmethacrylates). J. Biomed. Mater. Res. Symp. **6**: 89-98.

[14] Litsky AS, Rose RM, Rubin CT, Thrasher EL (1990) A reduced-modulus acrylic bone cement: Preliminary results. J. Orthop. Res. **8**: 623-626.

[15] Pilliar RM, Cameron HU, MacNab I (1975) Porous surface layered prosthetic devices. Biomed. Eng. **10**: 126-131.

[16] Pilliar RM, Blackwell R, McNab I, Cameron HU (1976) Carbon fiber-reinforced bone cement in orthopedic surgery. J. Biomed. Mater. Res. **10**: 893-906.

[17] Pourdeyhimi B, Robinson HH, Schwartz P, Wagner HD (1986) Fracture toughness of Kevlar 29/ poly (methylmethacrylate) composite materials for surgical implantations. Ann. Biomed. Eng. **14**: 277-294.

[18] Rimnac CM, Wright TM, McGill DL (1986) The effect of centrifugation on the fracture properties of acrylic bone cements. J. Bone Joint Surg. **68-A**: 281-287.

[19] Robinson RP, Wright TM, Burstein AH (1981) Mechanical properties of poly(methyl methacrylate) bone

Figure 7a

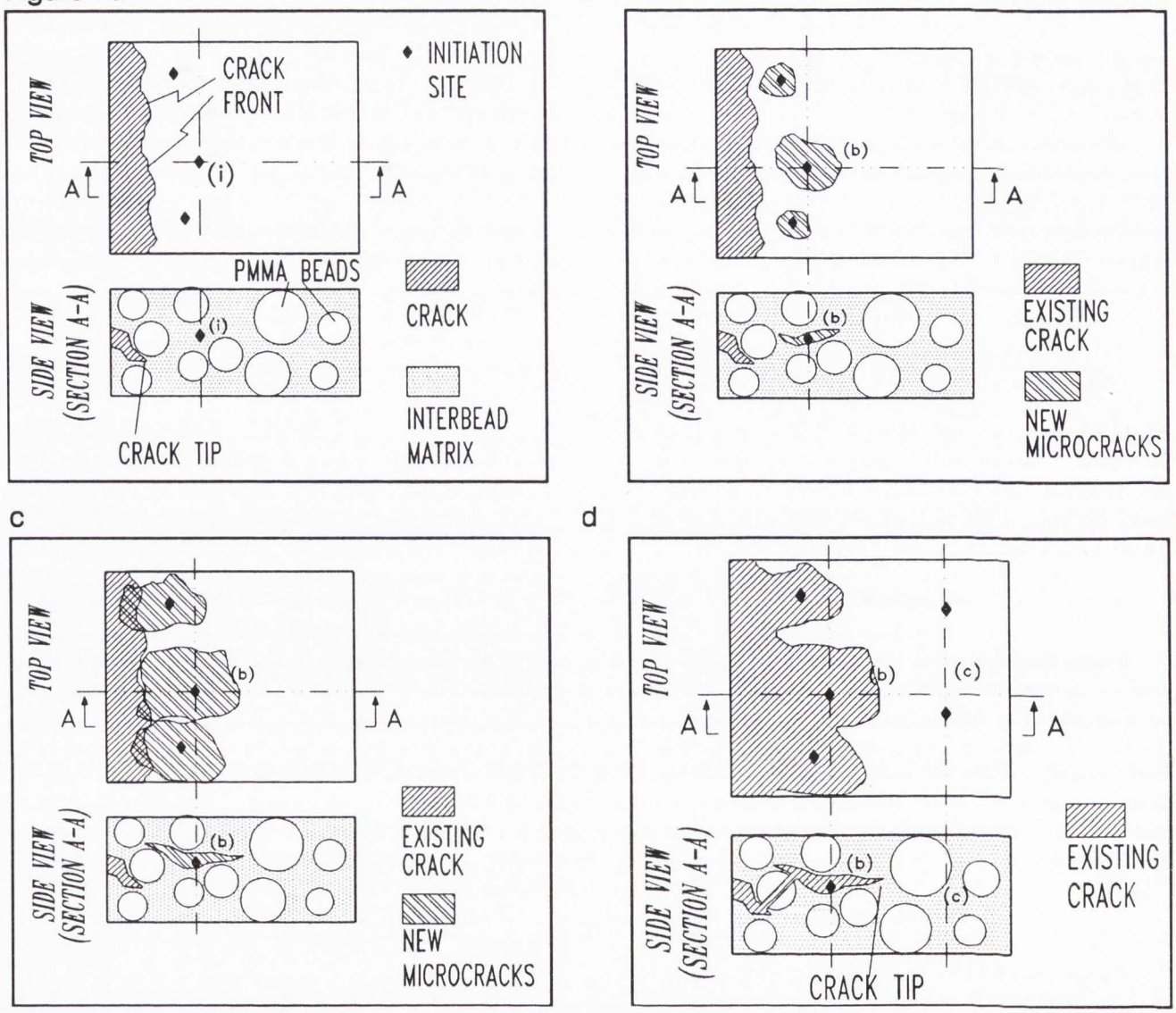

cements. J. Biomed. Mater. Res. **15**: 203-208.

[20] Saha S, Pal S (1984) Improvement of mechanical properties of acrylic bone cement by fiber reinforcement. J. Biomechanics **17**: 467-478.

[21] Topoleski LDT, Ducheyne P, Cuckler JM (1990) A fractographic analysis of *in vivo* poly(methyl methacrylate) bone cement failure mechanisms. J. Biomed. Mater. Res. **24**: 135-154.

[22] Topoleski LDT, Ducheyne P, Cuckler JM (1992) Fracture toughness of titanium fiber reinforced bone cement. J. Biomed. Mater. Res. **26**: 1599-1617.

[23] Topoleski LDT, Ducheyne P, Cuckler JM (1993) Microstructural pathway of fracture in poly(methyl methacrylate) bone cement. Biomaterials **14**: 1165-1172.

[24] Wang CT, Pilliar RM (1989) Fracture toughness of acrylic bone cements. J. Mater. Sci. **24**: 3725-3738.

Figure 7 (on the facing page). A model of three-dimensional fatigue crack propagation in bone cement. Depending on the state of the crack propagation, and the cross-section of the specimen observed in the SEM, different crack features would appear. (**a**). A crack front is propagating from left to right. Potential microcrack initiation sites exist ahead of the crack tip (indicated by black diamonds). In a cross sectional micrograph of A-A, only initiation site (i) would be seen. (**b**). Microcrack nucleation begins at the nucleation sites ahead of the crack tip. The nucleated cracks are roughly circular, or "penny shaped", in the commonly used fracture terminology. Only microcrack (b) can be seen in a micrograph taken of section A-A. (**c**). The nucleated microcracks grow radially, and appear to prefer to grow through the interbead matrix. Simultaneously the crack front may advance. Because the interbead matrix is porous compared to the beads - the porosity appears to be caused by the presence of the radiopacifier [23, 26] - the interbead matrix may have a lower fracture resistance (toughness) than the bead phase. In a micrograph through section A-A, it appears that the microcrack (b) is growing both forward and back toward the crack front. The crack front and the microcracks may appear to overlap in the top view, but when seen in profile, they may still be separated. (**d**). The original crack front and the microcracks coalesce, perhaps by cleaving a bead, and microcracks are forming at new initiation sites (black diamonds). Any microcracking starting at the site just below (c) would not appear in a micrograph taken at section A-A. (**e**). As the cycle continues (schematic "**e**" is comparable to "**b**"), the microcracks grow, and the lower microcrack intersects section A-A, and would now appear on a micrograph.

---

[25] Weightman B, Freeman MAR, Revell PA, Braden M, Albrektsson BEJ, Carlson LV (1987) The mechanical properties of cement and loosening of the femoral component of hip replacements. J. Bone Joint Surg. **69-B**: 558-564.

[26] Wright TM, Trent PS (1979) Mechanical properties of aramid fibre-reinforced acrylic bone cement. J. Mater. Sci. **14**: 503-505.

[27] Wright TM, Robinson RP (1982) Fatigue crack propagation in polymethylmethacrylate bone cements. J. Mater. Sci. **17**: 2463-2468.

Discussion with Reviewers

C.A. Scotchford: The authors state that images were difficult to focus at high magnification. This is surprising: one might expect a relatively planar surface to be achieved after polishing. Please comment.

Authors: Best BE images are obtained (on our SEM) when the specimen surface is at the smallest possible working distance. Focussing the image is achieved partly by adjusting the height of the specimen. The specimen is a polymer, and susceptible to beam damage (as evidenced on several of our micrographs). High magnification tended to destroy the specimen surface. Also, an increased spot size gives us better atomic number (Z) contrast. Unfortunately, a larger spot size also reduces the resolution of the SEM. Indeed, we produced a planar polished surface, which actually contributes to focussing difficulty. Topographic contrast aids in focussing.

C.A. Scotchford: In certain cases (e.g., Figure 5), the authors state that observed microcracks were discontinuous. As they are only observing a two-dimensional surface, can they be sure that these crack are indeed discontinuous in the third dimension?

Authors: Until something is observed, we can never be sure about it. In several other studies, and all throughout our work, we have observed discontinuous microcracks regardless of the polishing depth. We have also performed sequential polishing on single specimens to observe the crack front at different cross-sections, and we still see discontinuous microcracks. A schematic of a proposed model illustrates the possible three-dimensional characteristics of the crack propagation, showing how the cross-sectional micrographic characteristics are derived (Figure 7).

C.A. Scotchford: How close to crack propagation *in vivo* do you consider your model system to be, considering the differences in time scale and loading regimes and the presence of an active cellular environment?

Authors: The model is quite simple compared to the *in vivo* situation. Clearly, the *in vivo* boundary value problem is complex, with variable geometry and boundary conditions. In our model, we are trying to develop an understanding of the material's response to known boundary conditions, and thus,learn about the third critical component of a boundary value problem: the material properties. In a more complex experimental model, we might not be able to identify the variables responsible for material behaviors. The active cellular environment will most likely affect *in vivo* bone cement through bone remodeling. It is well known that bone geometry changes, probably depending on the applied stresses or strains. As the bone geometry changes, the boundary conditions, i.e., the loads on the bone cement, may also change. Clearly, this is not addressed in this study, but the information gained by these relatively simple experiments may be used to build more complex systems. It

may be that numerical methods, like finite element analysis, will be effective in analyzing the complex *in vivo* structure, and again, our studies will provide information essential for useful finite element models.

H. Demian: What is the origin of the big pore in Figure 6a? I think that it may have been a large agglomerate of $BaSO_4$. If this large agglomerate had cracked, then possibly the contents could have been discharged from the agglomerate. This would just leave the outer casing of a pore which contained the agglomerate. If you compare the inner contents of the two pores in Figure 6a, you see that the morphologies of the inner part of the pores are different. On one hand, the large pore is lined with $BaSO_4$ particles. On the other hand, the interior of the smaller pore seems to be very smooth. Whatever the origin of the pore is, it still is considered a pore, please comment.
Authors: The reviewer presents a logical argument that the pore may have initially been a $BaSO_4$ agglomerate. It may be that a small agglomerate of radiopacifier was the nucleation site of a pore, which expanded and pushed the $BaSO_4$ particles out with the pore's surface. It is hard to speculate further on the origin of the pore, and as the reviewer points out, from a mechanical perspective, a pore is still a pore, regardless of origin.

H. Demian: Have you been able to prove that the diamond saw-scalpel cut notches produce microcracks in the bone cement?
Authors: We have not proven, in an experimental sense, that the diamond saw-scalpel cut notches produce microcracks in every instance. We observed that in many of the specimens (about half), there were microcracks apparently originating at the corners of the saw-cut notches prior to fatigue loading. The presence or absence of the microcracks would not be known *a priori*, and thus, we felt that the technique was inappropriate for our fracture **initiation** studies in progress. Using the saw/scalpel-cutting technique would be fine for fracture toughness or fatigue crack propagation studies.

A. Litsky: Would you expect crack initiation of unnotched specimens to occur in the interbead region? Do you have any evidence that it does?
Authors: We would expect crack initiation of unnotched specimens in the interbead region, although, we have no evidence yet. The crack will initiate where the stresses or strain energy create conditions favorable for initiation. Because the microcracks seem to prefer the interbead matrix in the radiopaque bone cement, it is a logical assumption that even without a notch, microcracking, and hence crack initiation, will occur in the interbead material.

A. Litsky: You suggest that the radiopacifier in the interbead matrix may be the reason for the microcracking. Have you looked at any samples of radiolucent bone cement under similar conditions?
Authors: We have looked at radiolucent bone cement both in fatigue crack propagation and under conditions similar to those reported. The fatigue crack propagation of radiolucent bone cement are being reported in a separate paper (Molino LN, Topoleski LDT: The effect of $BaSO_4$ on the fatigue crack propagation rate of PMMA bone cement. J.Biomed. Mater. Res., in press). In the radiolucent bone cement, we observed that the crack propagates fairly straight and results in a flat fracture surface, as opposed to the tortuous crack path, and irregular surface of a crack propagating through radiopaque bone cement. It is difficult to differentiate the beads from the interbead matrix in the radiolucent cement, but if a crack propagates straight through the material, it must cleave beads and move through the matrix.

A. Brain: Charging caused problems by obscuring some of the microstructural details. Did you consider reducing the accelerating voltage for the SE examination to eliminate the problem?
Authors: We are constantly adjusting all parameters to obtain the most useful images possible. Because there are slight variations in specimen preparation, each specimen produces images differently. In our polished specimens, the radiopacifier is actually mostly below the surface (much like an iceberg). The higher the incident beam voltage, the greater the electron penetration into the surface, and the more secondary and backscattered electrons are liberated from the radiopacifier, giving a clearer image. We are still exploring the effect of voltage on the imaging of the radiopacifier. Charging of the specimen is desired, in a way, because it is the charging on the edge of the crack that makes it easy to distinguish the crack. Therefore, we are constantly adjusting the beam voltage to show specific specimen attributes as the need arises. Many times we will take several images of the same area with different voltages.